Molecular Medicine

RESEARCH ARTICLE

Open Access

Gut microbiota-testis axis: FMT improves systemic and testicular micro-environment to increase semen quality in type 1 diabetes

Yanan Hao[1,2,3†], Yanni Feng[4†], Xiaowei Yan[1,2†], Liang Chen[1†], Ruqing Zhong[1†], Xiangfang Tang[1], Wei Shen[2], Qingyuan Sun[5], Zhongyi Sun[6], Yonglin Ren[3], Hongfu Zhang[1,3*] and Yong Zhao[1,3*]

Abstract

Background: Clinical data suggest that male reproductive dysfunction especially infertility is a critical issue for type 1 diabetic patient (T1D) because most of them are at the reproductive age. Gut dysbiosis is involved in T1D related male infertility. However, the improved gut microbiota can be used to boost spermatogenesis and male fertility in T1D remains incompletely understood.

Methods: T1D was established in ICR (CD1) mice with streptozotocin. Alginate oligosaccharide (AOS) improved gut microbiota (fecal microbiota transplantation (FMT) from AOS improved gut microbiota; A10-FMT) was transplanted into the T1D mice by oral administration. Semen quality, gut microbiota, blood metabolism, liver, and spleen tissues were determined to investigate the beneficial effects of A10-FMT on spermatogenesis and underlying mechanisms.

Results: We found that A10-FMT significantly decreased blood glucose and glycogen, and increased semen quality in streptozotocin-induced T1D subjects. A10-FMT improved T1D-disturbed gut microbiota, especially the increase in small intestinal *lactobacillus*, and blood and testicular metabolome to produce n-3 polyunsaturated fatty acid (PUFA) docosahexaenoic acid (DHA) and eicosapentaenoic acid (EPA) to ameliorate spermatogenesis and semen quality. Moreover, A10-FMT can improve spleen and liver functions to strengthen the systemic environment for sperm development. FMT from gut microbiota of control animals (Con-FMT) produced some beneficial effects; however, to a smaller extent.

Conclusions: AOS-improved gut microbiota (specific microbes) may serve as a novel, promising therapeutic approach for the improvement of semen quality and male fertility in T1D patients via gut microbiota-testis axis.

Keywords: Type 1 diabetes, A10-FMT, Blood glucose, Semen quality, DHA, EPA

Introduction

Type 1 diabetes (T1D), one of the most common metabolic disorders in children and young adults, is a multifactorial, immune-mediated disease that is characterized by the progressive destruction of autologous insulin-producing beta cells in the pancreas, and an increase in blood glucose levels (hyperglycemia Barkabi-Zanjani et al. 2020; Mariño et al. 2017; Gülden et al. 2015). Diabetic hyperglycemia leads to further disorder, including cardiovascular disease, neuropathy, nephropathy, retinopathy,

*Correspondence: zhanghongfu@caas.cn; yzhao818@hotmail.com; Yong.Zhao@murdoch.edu.au
†Yanan Hao, Yanni Feng, Xiaowei Yan, Liang Chen, and Ruqing Zhong have contributed equally
[1] State Key Laboratory of Animal Nutrition, Institute of Animal Sciences, Chinese Academy of Agricultural Sciences, Beijing 100193, People's Republic of China
Full list of author information is available at the end of the article

and male impotence. Moreover, hyperglycemia-induced reproductive dysfunction has been reported in most T1D studies with male patients (Maresch et al. 2018). This increase in diabetes in young persons is of great concern as it will increase fertility related disorders during their reproductive lifespan (La Vignera et al. 2015). Furthermore, the frequency of diabetes mellitus (DM) in males is higher than in females, and the incidence of infertility among diabetic males is more common, which likely contributes to the reduction of global birth rates and fertility (Maresch et al. 2018). Many investigations have found DM-induced male infertility at multiple levels, such as changes in spermatogenesis, testes, ejaculatory function and libido (La Vignera et al. 2015; Jangir and Jain 2014). Additionally, cross-sectional studies reported that at the time of infertility diagnosis, young men are already less healthy than their fertile peers which suggests that male reproductive and somatic health are tightly corelated (Glazer et al. 2017).

Although T1D has a strong genetic basis, epigenetic and environmental factors (hygiene, antibiotic use, and diet) are involved in its development (de Groot et al. 2021; Gülden et al. 2015). Furthermore, all of these potential environmental risk factors are related to the intestine and its microbiota. Specific alterations in the diversity of intestinal microflora have been reported to be one characteristic of diabetic patients by the epidemiological investigations (Li et al. 2020; Abdellatif et al. 2019; Neuman et al. 2019). Interaction of the gut microbes with the innate immune system plays vital roles in the development of T1D (de Groot et al. 2021). It has been reported that a reduction in bacterial and functional diversity, and community stability are found in preclinical T1D patients, on the other hand *Bacteroidetes* is dominated (Knip and Honkanen 2017; Knip and Siljander 2016; Kostic et al. 2015; Wen et al. 2008). The presence of small intestinal *Prevotella* is known to be inversely related to pancreatic beta cell function, however small intestinal *Desulfovibrio* are involved in preserved beta cell function (de Groot et al. 2021).

Very recently, it has been established that the gut microbiota plays crucial roles in spermatogenesis and male fertility (Zhang et al. 2021a, 2021b, 2022; Ding et al. 2020). Studies demonstrate a strong link between testicular function and the regulation of gut microbiota via host metabolomes, as beneficial microbiota have been shown to significantly improve busulfan impaired spermatogenesis and semen quality (Zhang et al. 2021a, b). Since noting the high incidence of infertility in T1D male patients, many investigators have tried to improve the semen quality and fertility in T1D induced animal models (Liu et al. 2019; Simas et al. 2017). It is reported that resveratrol attenuates reproductive alterations in T1D-induced rats with improvements in glycemic level, sperm quantitative and qualitative parameters, and the hormonal profile (Simas et al. 2017). Liu et al. found that metformin ameliorates testicular damage (90% of male DM patients have varying degrees of testicular dysfunction) in male mice with streptozotocin (STZ)-induced T1D through the PK2/PKR pathway (Liu et al. 2019). In our previous studies, we found that alginate oligosaccharide (AOS) could benefit gut microbiota to promote spermatogenesis in busulfan treated mice (Zhao et al. 2020). And AOS benefited gut microbiota transplanted into busulfan treated animals (fecal microbiota transplantation; FMT) to boost the spermatogenesis and increase semen quality (Zhang et al. 2021a, b). FMT, a key novel therapeutic approach, can restore an upset gut microbiota to a premorbid state; this has been shown in clinical and research studies (Allegretti et al. 2019). Furthermore, the application of FMT in fertility studies is an emerging novel approach (Yurtdaş and Akdevelioğlu 2019). However, it is unknown whether impaired spermatogenesis and semen quality in the T1D condition can be improved by FMT or specific microbes. Therefore, this study aimed to explore possible improvements in spermatogenesis and semen quality made by AOS benefited microbiota.

Materials and methods

Study design

All animal procedures used in this study were approved by the Animal Care and Use Committee of the Institute of Animal Sciences of Chinese Academy of Agricultural Sciences (IAS2020-106). Mice were maintained in specific pathogen-free (SPF) environment under a light: dark cycle of 12:12 h, at a temperature of 23 ℃ and humidity of 50–70%; they had free access to food (chow diet) and water (Zhang et al. 2021a, b; Zhao et al. 2020).

Experiment I: Mouse small intestine microbiota collection (Zhang et al. 2021a, b)

Three-week-old ICR male mice were dosed with ddH_2O as the control or AOS 10 mg/kg BW via oral gavage (0.1 ml/mouse/day). AOS dosing solution was freshly prepared on a daily basis and delivered every morning for three weeks. There were two groups (30 mice/treatment): (1) Control (ddH_2O); (2) A10 (AOS 10 mg/kg BW). After three weeks treatment, the animals were maintained on regular diet for three more days (no treatment). Then the mice were humanely euthanized to collect small intestinal luminal content (microbiota).

Experiment II: STZ treatment and microbiota transplants (FMT) (Zhang et al. 2021a,b; Bárcena et al. 2019; Brunse et al. 2019)

The small intestine luminal content (microbiota) from each group was pooled and homogenized, diluted 1:1

in 20% sterile glycerol (saline) and frozen. Before inoculation, fecal samples were diluted in sterile saline to a working concentration of 0.05 g/ml and filtered through a 70-μm cell strainer. Five-week-old ICR male mice were used in current investigation. There were four treatment groups (30 mice/treatment): (1) Control (Regular diet plus Saline); (2) STZ (One dose STZ at 135 mg/kg body weight after preliminary screening) (Simas et al. 2017); (3) Con-FMT [STZ plus gut microbiota from control mice (Experiment I)]; (4) A10-FMT [STZ plus gut microbiota from AOS 10 mg/kg mice (Experiment I)]. STZ was injected at the beginning of the experiment. Then the mice were received oral FMT inoculations (0.1 ml) once daily for two weeks (5 weeks of age to 7 weeks of age), and regularly maintained (on respective diet) for another 3 weeks (10 weeks of age). At the end of experiment, the mice were humanely euthanized to collect samples for different analyses (Fig. 1a; Study scheme).

Evaluation of spermatozoa motility using a computer-assisted sperm analysis system

Spermatozoa motility was assessed using a computer-assisted sperm assay (CASA) method according to World Health Organization guidelines (Zhao et al. 2020). After euthanasia, spermatozoa were collected from the cauda epididymis of mice and suspended in DMEM/F12 medium with 10% FBS and incubated at 37.5 ℃ for 30 min; samples were then placed in a pre-warmed counting chamber. The micropic sperm class analyzer (CASA system) was used in this investigation. It was equipped with a 20-fold objective, a camera adaptor (Eclipse E200, Nikon, Japan), and a camera (acA780-75gc, Basler, Germany), and it was operated by an SCA sperm class analyzer (MICROPTIC S.L.). The classification of sperm motility was as follows: grade A linear velocity > 22 μm s^{-1}; grade B < 22 μm s^{-1} and curvilinear velocity > 5 μm s^{-1}; grade C curvilinear velocity < 5 μm s^{-1}; and grade D = immotile spermatozoa. The spermatozoa motility data represented only grade A + grade B since only these two grades are considered to be functional.

Morphological observations of spermatozoa

The extracted murine caudal epididymides were placed in RPMI medium, finely chopped, and then Eosin Y (1%) was added for staining as described previously (Zhao et al. 2020). Spermatozoon abnormalities were then viewed using an optical microscope and were classified into head or tail morphological abnormalities: two heads, two tails, blunt hooks, and short tails. The examinations were repeated three times, and 500 spermatozoa per animal were scored.

Assessment of acrosome integrity

After harvest, mouse spermatozoa were incubated at 37.5 ℃ for 30 min, after which a drop of sperm suspension was uniformly smeared on a clean glass slide. Smeared slides were air dried and incubated in methanol for 2 min for fixation. After fixation, the slides were washed with PBS three times. Assessment of an intact acrosome was accomplished by staining the sperm with 0.025% Coomassie brilliant blue G-250 in 40% methanol for 20 min at room temperature (RT). The slides were then washed three times with PBS and mounted with 50% glycerol in PBS. Acrosomal integrity was determined by an intense staining on the anterior region of the sperm head under bright-field microscopy (AH3-RFCA, Olympus, Tokyo, Japan) and scored accordingly (Zhao et al. 2020).

RNA Isolation and RNA-seq analyses (Zhao et al. 2020)

Briefly, total RNA was isolated using TRIzol Reagent (Invitrogen) and purified using a Pure-Link1 RNA Mini Kit (Cat: 12183018A; Life Technologies) following the manufacturers' protocol. Total RNA samples were first treated with DNase I to degrade any possible DNA contamination. Then the mRNA was enriched using oligo(dT) magnetic beads. Mixed with the fragmentation buffer, the mRNA was broken into short fragments (about 200 bp), after which, the first strand of cDNA was synthesized using a random hexamer-primer. Buffer, dNTPs, RNase H, and DNA polymerase I were added to synthesize the second strand. The double strand cDNA was purified with magnetic beads. Subsequently, 3′-end single nucleotide A (adenine) addition was performed. Finally, sequencing adaptors were ligated to the fragments. The fragments were enriched by PCR amplification. During the QC step, an Agilent 2100 Bioanaylzer and ABI StepOnePlus Real-Time PCR System were used to qualify and quantify the sample library. The library products were prepared for sequencing in an Illumina

(See figure on next page.)

Fig. 1 A10-FMT decreased blood glucose, and improved semen quality in type 1 diabetes. **a** Blood glucose levels. The y-axis represents the concentration. The x-axis represents the treatment (n = 30/group). *$p < 0.05$. **b** Blood glycogen levels. The y-axis represents the relative amount. The x-axis represents the treatment (n = 30/group). *$p < 0.05$. **c** Sperm concentration. The y-axis represents the concentration. The x-axis represents the treatment (n = 30/group). *$p < 0.05$. **d** Sperm motility. The y-axis represents the percentage of cells. The x-axis represents the treatment (n = 30/group). *$p < 0.05$

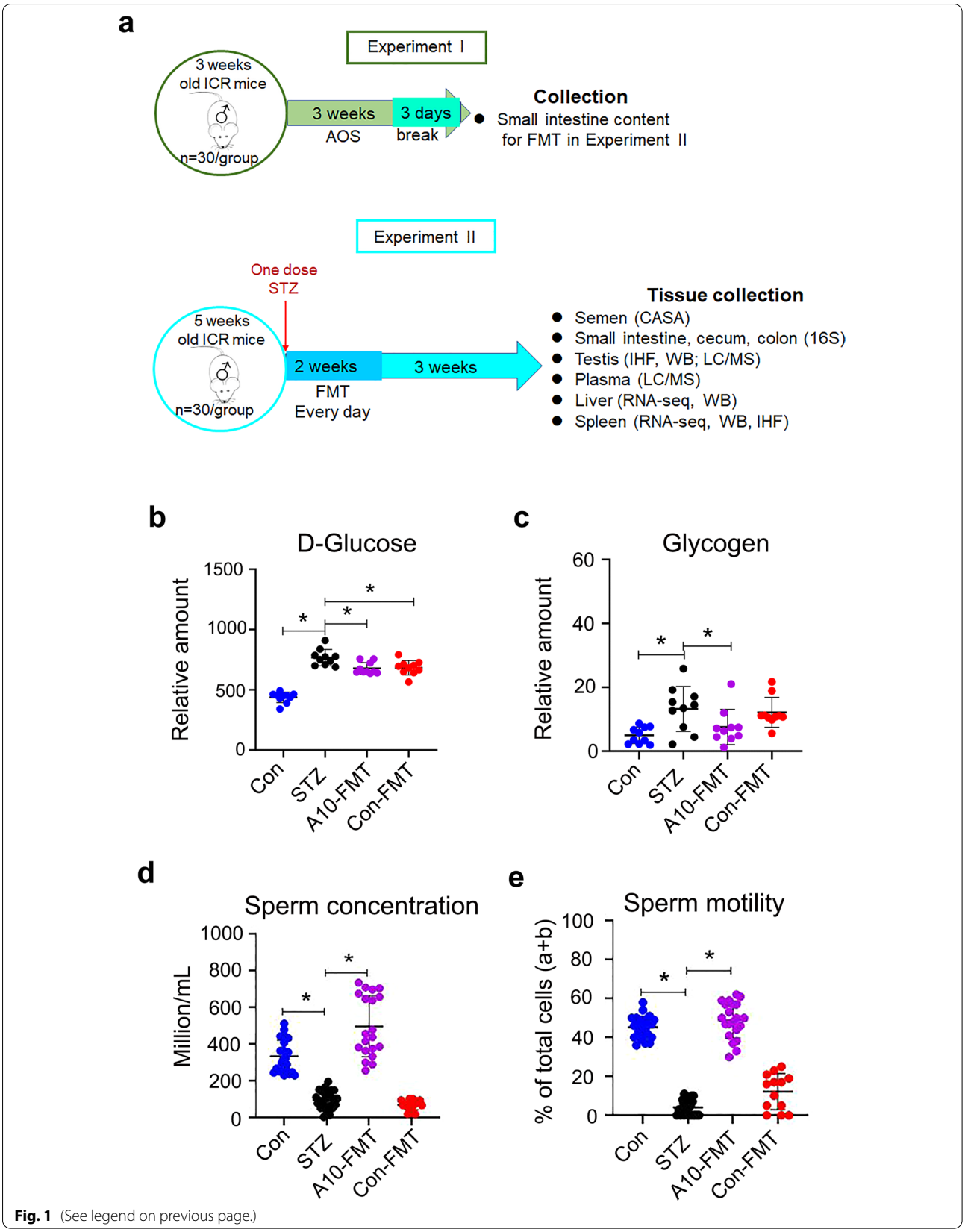

Fig. 1 (See legend on previous page.)

HiSeqTM 2500. The reads were mapped to reference genes using SOAPaligner (v. 2.20) with a maximum of two nucleotide mismatches allowed at the parameters of "-m 0- × 1000 -s 40 -l 35 -v 3 -r 2". The read number of each gene was transformed into RPKM (reads per kilo bases per million reads), and then differentially expressed genes were identified using the DEGseq package and the MARS (MA-plot-based method with random sampling model) method. The threshold was set as FDR ≤ 0.001 and an absolute value of $\log_2$ ratio ≥ 1 to judge the significance of the difference in gene expression. Then on the data were analyzed by GO enrichment, KEGG enrichment.

Sequencing of microbiota from intestine digesta samples and data analysis (Zhao et al. 2020)

DNA extraction Total genomic DNA of small intestine, cecum and colon digesta was isolated using an E.Z.N.A.R Stool DNA Kit (Omega Bio-tek Inc., USA) following the manufacturer's instructions. DNA quantity and quality were analyzed using NanoDrop 2000 (Thermo Scientific, USA) and 1% agarose gel. Ten samples/groups were determined.

Library preparation and sequencing The V3-V4 region of the 16S rRNA gene was amplified using the primers MPRK341F (50-ACTCCTACGGGAGGCAGCAG-30) and MPRK806R: (50-GGACTACHVGGGTWTCTAAT-30) with Barcode. The PCR reactions (total 30 μL) included 15 μL PhusionR High-Fidelity PCR Master Mix (New England Biolabs), 0.2 mM primers, and 10 ng DNA. The thermal cycle was carried out with an initial denaturation at 98 ℃, followed by 30 cycles of 98 ℃ for 10 s, 50 ℃ for 30 s, 72 ℃ for 30 s, and a final extension at 72 ℃ for 5 min. PCR products were purified using a GeneJET Gel Extraction Kit (Thermo Scientific, USA). The sequencing libraries were constructed with NEB NextR UltraTM DNA Library Prep Kit for Illumina (NEB, United States) following the manufacturer's instructions and index codes were added. Then, the library was sequenced on the Illumina HiSeq 2500 platform and 300 bp paired-end reads were generated at the Novo gene. The paired-end reads were merged using FLASH (V1.2.71). The quality of the tags was controlled in QIIME (V1.7.02), meanwhile all chimeras were removed. The "Core Set" of the Greengenes database3 was used for classification, and sequences with > 97% similarity were assigned to the same operational taxonomic units (OTUs).

Analysis of sequencing data Operational taxonomic unit abundance information was normalized using a standard of sequence number corresponding to the sample with the least sequences. The alpha diversity index was calculated with QIIME (Version 1.7.0). The Unifrac distance was obtained using QIIME (Version 1.7.0), and PCoA (principal coordinate analysis) was performed using R software (Version 2.15.3). The linear discriminate analysis effect size (LEfSe) was performed to determine differences in abundance; the threshold LDA score was 4.0. GraphPad Prism7 software was used to produce the graphs.

Plasma and testis metabolite measurements by LC–MS/MS

Plasma samples were collected and immediately stored at − 80 °C. Before LC–MS/MS analysis, the samples were thawed on ice and processed to remove proteins. Testis samples were collected and the same amount of tissue from each mouse testis was used to isolate the metabolites using CH_3OH:H_2O (V:V) = 4:1. Then samples were detected by ACQUITY UPLC and AB Sciex Triple TOF 5600 (LC/MS) as reported previously (Zhang et al. 2021a,b). Ten samples/groups were analyzed for plasma or testis samples. The HPLC conditions employed an ACQUITY UPLC BEH C18 column (100 mm × 2.1 mm, 1.7 μm), solvent A [aqueous solution with 0.1% (v/v) formic acid], and solvent B [acetonitrile with 0.1% (v/v) formic acid] with a gradient program. The flow rate was 0.4 ml/min and the injection volume was 5 μl. Progenesis QI v2.3 (Nonlinear Dynamics, Newcastle, UK) was implemented to normalize the peaks. Then the Human Metabolome Database (HMDB), Lipidmaps (v2.3), and METLIN software were used to qualify the data. Moreover, the data were processed with SIMCA software (version 14.0, Umetrics, Umeå, Sweden) following pathway enrichment analysis using the KEGG database (http://www.genome.jp/KEGG/pathway.html).

Determination of blood glucose, insulin, ALT, TG, TC, T-AOC, GSH, SOD and catalase

Blood insulin was determined by the kit form Beijing Solarbio Science & Technology Co., Ltd (Beijing, P. R. China; Cat. #: SEKM0141). Blood glucose, ALT, TG, TC, T-AOC, SOD, and catalase were determined by the kits from Nanjing Jiancheng Bioengineering Institute [Nanjing, P.R. China; glucose (Cat. #: F006-1-1); ALT (Cat. #: C009-2-1); TG (Cat. #: A110-1-1); TC (Cat. #: A111-1-1); T-AOC (Cat. #: A015-2-1); GSH (Cat. #: A006-2-1); SOD (Cat. #: A001-3-2); Catalase (Cat. #: A007-1-1)] (Chu et al. 2018). All the procedures were followed from the manufacturer's instructions.

Measurement of iron content in spleen

The amount of ferric iron in the spleens was determined by Perl's Prussian blue stain as described by Kohyama et al (2009). Spleen tissues were fixed with 4% paraformaldehyde, then embedded in paraffin. And 5 μm sections were cut and stained with Perl's Prussian blue and pararosaniline (Sigma).

Histopathological analysis

Testicular tissues were fixed in 10% neutral buffered formalin, paraffin embedded, cut into 5 µm sections and subsequently stained with hematoxylin and eosin (H&E) for histopathological analysis.

Western blotting

Western blotting analysis of proteins was carried out as previously reported (Zhang et al. 2021a; Zhao et al. 2020). Briefly, testicular tissue samples were lysed in RIPA buffer containing the protease inhibitor cocktail from Sangong Biotech, Ltd. (Shanghai, China). Protein concentration was determined using a BCA kit (Beyotime Institute of Biotechnology, Shanghai, China). Goat anti-actin was used as a loading control. The information for primary antibodies (Abs) were listed in Additional file 1: Table S1. Secondary donkey anti-goat Ab (Cat no.: A0181) was purchased from Beyotime Institute of Biotechnology, and goat anti-rabbit (Cat no.: A24531) Abs were bought from Novex® by Life Technologies (USA). Fifty micrograms of total protein per sample were loaded onto 10% SDS polyacrylamide electrophoresis gels. The gels were transferred to a polyvinylidene fluoride (PVDF) membrane at 300 mA for 2.5 h at 4 ℃. The membranes were then blocked with 5% bovine serum albumin (BSA) for 1 h at RT, followed by three washes with 0.1% Tween-20 in TBS (TBST). The membranes were incubated with primary Abs diluted with 1:500 in TBST with 1% BSA overnight at 4 ℃. After three washes with TBST, the blots were incubated with the HRP-labelled secondary goat anti-rabbit or donkey anti-goat Ab respectively for 1 h at RT. After three washes, the blots were imaged. The bands were quantified using Image-J software. The intensity of the specific protein band was normalized to actin first, then the data were normalized to the control. The experiment was repeated > 6 times.

Detection of protein levels and location in testis using immunofluorescence staining

The methodology for immunofluorescence staining of testicular samples is reported in our recent publications (Zhang et al. 2021a; Zhao et al. 2020). Sections of testicular tissue (5 µm) were prepared and subjected to antigen retrieval and immunostaining as previously described (Zhang et al. 2021a; Zhao et al. 2020). Briefly, sections were first blocked with normal goat serum in PBS, followed by incubation with primary Abs (Additional file 1: Table S1; 1:100 in PBS-0.5% Triton X-100; Bioss Co. Ltd. Beijing, PR China) at 4 °C overnight. After a brief wash, sections were incubated with an Alexa 546-labeled goat anti-rabbit secondary Ab (1:100 in PBS; Molecular Probes, Eugene, OR, USA) at RT for 30 min and then counterstained with 4′,6-diamidino-2-phenylindole (DAPI). The stained sections were examined using a Leica Laser Scanning Confocal Microscope (LEICA TCS SP5 II, Germany). Ten animal samples from each treatment group were analysed. Positively stained cells were counted. A minimum of 1000 cells were counted for each sample of each experiment. The data were then normalized to the control.

Statistical analysis

Data were analyzed using SPSS statistical software (IBM Co., NY) with one-way analysis of variance (ANOVA) followed by LSD multiple comparison tests or T-test. The data were shown as the mean ± SEM. Statistical significance was based on $p < 0.05$.

Results

A10-FMT decreased blood glucose, ameliorated STZ-induced T1D diminished semen quality, and impaired gut microbiota

Three days after STZ treatment (one dose, 135 mg/kg body weight), blood glucose was significantly higher in the STZ group [23.8 ± 2.1 mmol/l (mM)] than that in the control group (Con; 8.2 ± 1.3 mM) which indicated that the animals were diabetic (T1D; Fig. 1a; Study scheme). After five weeks treatment, the body weight and blood insulin were lower in STZ group than that in Con, while FMT from AOS improved gut microbiota (A10-FMT) produced a slight increase in body weight and blood insulin over STZ [no significant difference between STZ, A10-FMT, and FMT from gut microbiota of control animals (Con-FMT); Additional file 2: Fig. S1a and b]. After five weeks of treatment, blood glucose was significantly higher in STZ while it was significantly decreased by A10-FMT and Con-FMT (Fig. 1b). At the same time blood glycogen was higher in STZ animals while it was significantly reduced by A10-FMT but not Con-FMT (Fig. 1c). STZ significantly diminished semen quality through decreasing sperm motility and concentration (Fig. 1d and e). However, A10-FMT significantly increased sperm motility and concentration, while Con-FMT produced a slight change (Not significantly; Fig. 1d and e).

Gut dysbiosis has been reported in both T1D humans and animal models (Li et al. 2020; Abdellatif et al. 2019; Neuman et al. 2019). Moreover, dysbiosis may also impair spermatogenesis to decrease semen quality (Ding et al. 2020). In the current investigation, we found a similar phenomenon as the microbiota in the small intestine, cecum, and colon were changed in T1D animals with an increase in the harmful bacteria *Mycoplasma,* and *Escherichia* (Fig. 2a–d; Additional file 2: Fig. S1c–n, Fig. S2; de Groot et al. 2021; Knip and Siljander 2016). A10-FMT increased the beneficial microbiota *Lactobacillus* in

the small intestine, while decreasing the harmful bacteria *Escherichia* in the cecum and colon (Fig. 2a–d; Additional file 2: Fig. S1c–n, Fig. S2). However, Con-FMT decreased *Bacteroides*, *Mycoplasma,* and *Escherichia,* but did not increase *Lactobacillus* (Fig. 2a–d; Additional file 2: Fig. S1c–n, Fig. S2).

The gut microbiota participates in host metabolism by interacting with host signaling pathways. Kyoto Encyclopedia of Genes and Genomes (KEGG) analysis of changed microbiota genes found that 12 major signaling pathways were upset by STZ and recovered by A10-FMT and/or Con-FMT in the intestine (Fig. 2e). Interestingly, the "biosynthesis of other secondary metabolites" pathway was increased by A10-FMT specifically in the colon, and the "energy metabolism" pathway was decreased by STZ while increased by A10-FMT in the colon; meanwhile, the "carbohydrate metabolism" pathway was increased by A10-FMT while decreased by Con-FMT in the small intestine (Fig. 2e). Moreover, the "Energy metabolism" pathway in the cecum, "amino acid metabolism" pathway in the small intestine, and "metabolism of cofactor and vitamins" pathway in the small intestine were decreased by both A10-FMT and Con-FMT, while they were not changed by STZ; "membrane transport" pathway in the cecum, and "metabolism of other amino acids" and "lipid metabolism" in the small intestine were increased by both A10-FMT and Con-FMT while they remained unchanged by STZ; "xenobiotics biodegradation and metabolism" was decreased by STZ while increased by both A10-FMT and Con-FMT (Fig. 2e).

A10-FMT-recovered gut microbiota improved the blood metabolome

T1D is a metabolic related disease, and gut microbiota influence the blood metabolome; therefore, we next explored blood metabolite changes using LC/MS (Additional file 3: Data Set 1). KEGG enrichment analysis of changed microbiota genes indicated that the "carbohydrate metabolism" pathway was increased by A10-FMT in the small intestine, and it was interesting to note that blood carbohydrate was increased by STZ while decreased by A10-FMT or Con-FMT (Fig. 3a). Two other large clusters of compounds were decreased by STZ while increased by A10-FMT including flavonoids (Fig. 3b–d; Additional file 2: Fig. S3a), and glycerophosphocholines/glycerophospho- ethanolamines (Fig. 3e–h; Additional file 2: Fig. S3b–i).

In addition, melatonin, that has antioxidant effects along with many other functions, was decreased by STZ while increased by A10-FMT and Con-FMT (Fig. 3i) although at non-significant levels. L-carnitine, an important compound involved in male sperm formation and function, was decreased by STZ while significantly increased by A10-FMT but not by Co-FMT (Fig. 3j) which suggested that A10-FMT and Con-FMT differentially influence blood metabolites especially for antioxidant compound production. The data were consistent with gut microbiota data that A10-FMT increased *Lactobacillus* which have been shown to produce metabolites that improve liver or cardiac impairment (Lew et al. 2020; Wang et al. 2019; Malik et al. 2018) (Fig. 2e). Most interestingly, blood n-3 polyunsaturated acid (PUFA) eicosapentaenoic acid (EPA) was decreased by STZ while increased by A10-FMT and Con-FMT (Fig. 3k).

A10-FMT-improved blood metabolite ameliorated testicular metabolome (PUFA and retinoic acid) and the testicular microenvironment

The blood metabolites were upset in T1D (by STZ) while recovered under treatment with A10-FMT and/or Con-FMT. The blood metabolome and testicular metabolome are connected together, therefore, we set out to determine the testicular metabolome using LC/MS. It was notable that the testicular n-3 PUFAs DHA and EPA were significantly increased by A10-FMT but not by Con-FMT (Fig. 4a and b; Additional file 2: Fig. S4a and b; Additional file 3: Data Set 2). The retinoic acid pathway plays a crucial role in spermatogenesis (Griswold 2016; Bowles et al. 2006); and PUFA and retinoic acid signaling interact together to regulate spermatogenesis (Wolf 2006; Lengqvist et al. 2004). STZ decreased retinol or retinoic acid related compounds while A10-FMT increased them (Fig. 4c and e; Additional file 2: Fig. S4c–f) which suggested that spermatogenesis was initiated by A10-FMT since retinoic acid turns meiosis on. Moreover, the protein levels of the spermatogonia cell marker genes PLZF

(See figure on next page.)

Fig. 2 A10-FMT improved small intestinal and cecal microbiota in type 1 diabetes. **a** PLS-DA (OTU) of small intestine microbiota in HFD, A10-FMT, and Con-FMT groups. **b** Small intestine microbiota levels at the genus level in STZ, A10-FMT, and Con-FMT groups. The y-axis represents the relative amount (%). The x-axis represents the treatments. Different colors represent different microbiota. **c** Cladogram of the linear discriminate analysis effect size (LEfSe) determining the difference in abundance of small intestine microbiota. **d** Changed microbiota in the small intestine. The y-axis represents the relative amount at the genus level. The x-axis represents the treatment. *$p < 0.05$. **e** Summary of signaling pathways of changed microbiota genes by Kyoto Encyclopedia of Genes and Genomes (KEGG) enrichment analysis. Red arrow indicates increased microbiota genes in each comparison. Blue arrow indicates decreased microbiota genes in each comparison. N = 10/group

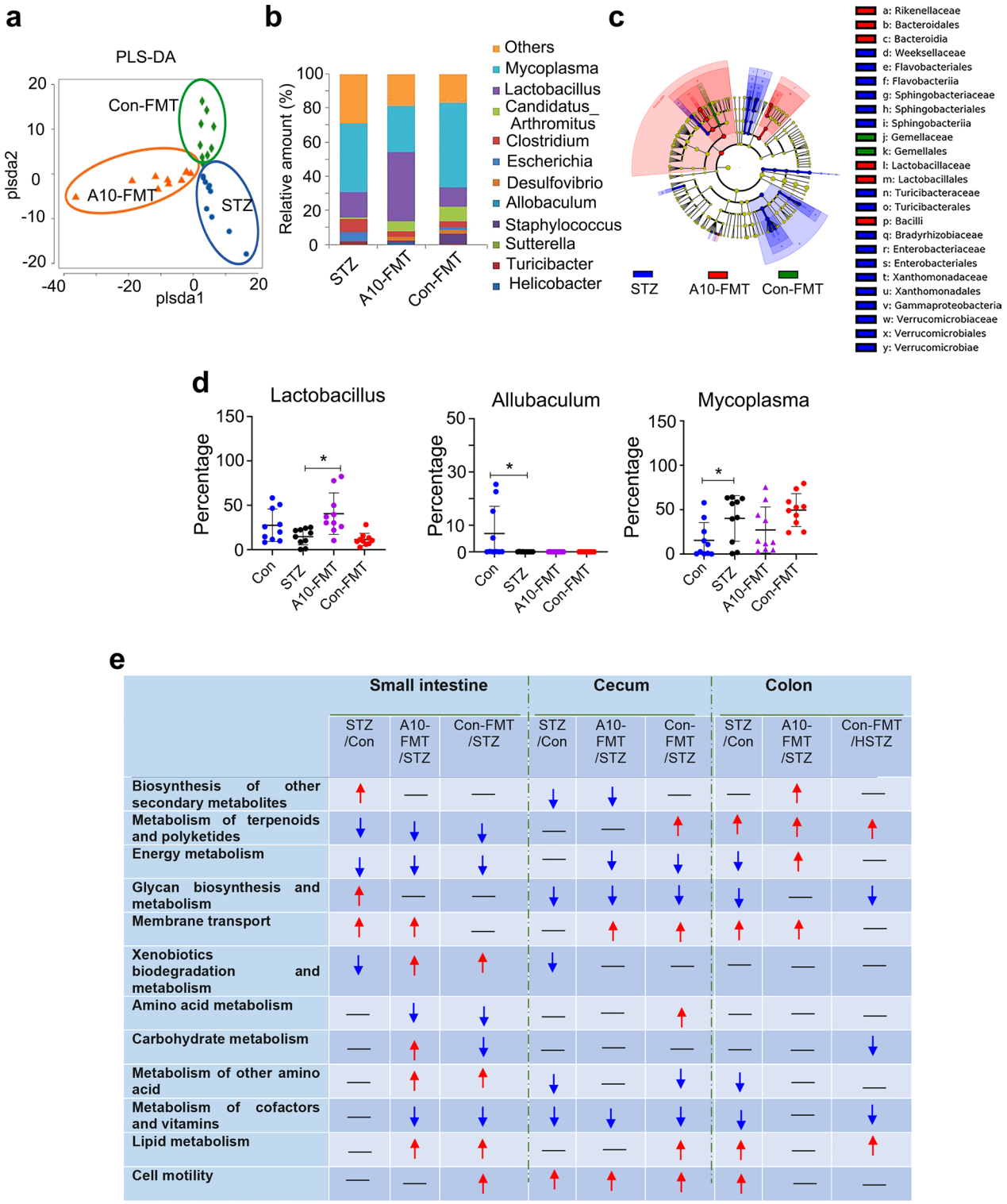

e

	Small intestine			Cecum			Colon		
	STZ /Con	A10-FMT /STZ	Con-FMT /STZ	STZ /Con	A10-FMT /STZ	Con-FMT /STZ	STZ /Con	A10-FMT /STZ	Con-FMT /HSTZ
Biosynthesis of other secondary metabolites	↑	—	—	↓	↓	—	—	↑	—
Metabolism of terpenoids and polyketides	↓	↓	↓	—	—	↑	↑	↑	↑
Energy metabolism	↓	↓	↓	—	↓	↓	↓	↑	—
Glycan biosynthesis and metabolism	↑	—	—	↓	↓	↓	↓	—	↓
Membrane transport	↑	↑	—	—	↑	↑	↑	↑	—
Xenobiotics biodegradation and metabolism	↓	↑	↑	↓	—	—	—	—	—
Amino acid metabolism	—	↓	↓	—	—	↑	—	—	—
Carbohydrate metabolism	—	↑	↓	—	—	—	—	—	↓
Metabolism of other amino acid	—	↑	↑	↓	—	↓	↓	—	—
Metabolism of cofactors and vitamins	—	↓	↓	↓	↓	↓	↓	—	↓
Lipid metabolism	—	↑	↑	—	—	↑	↑	—	↑
Cell motility	—	—	↑	↑	↑	↑	↑	—	—

Fig. 2 (See legend on previous page.)

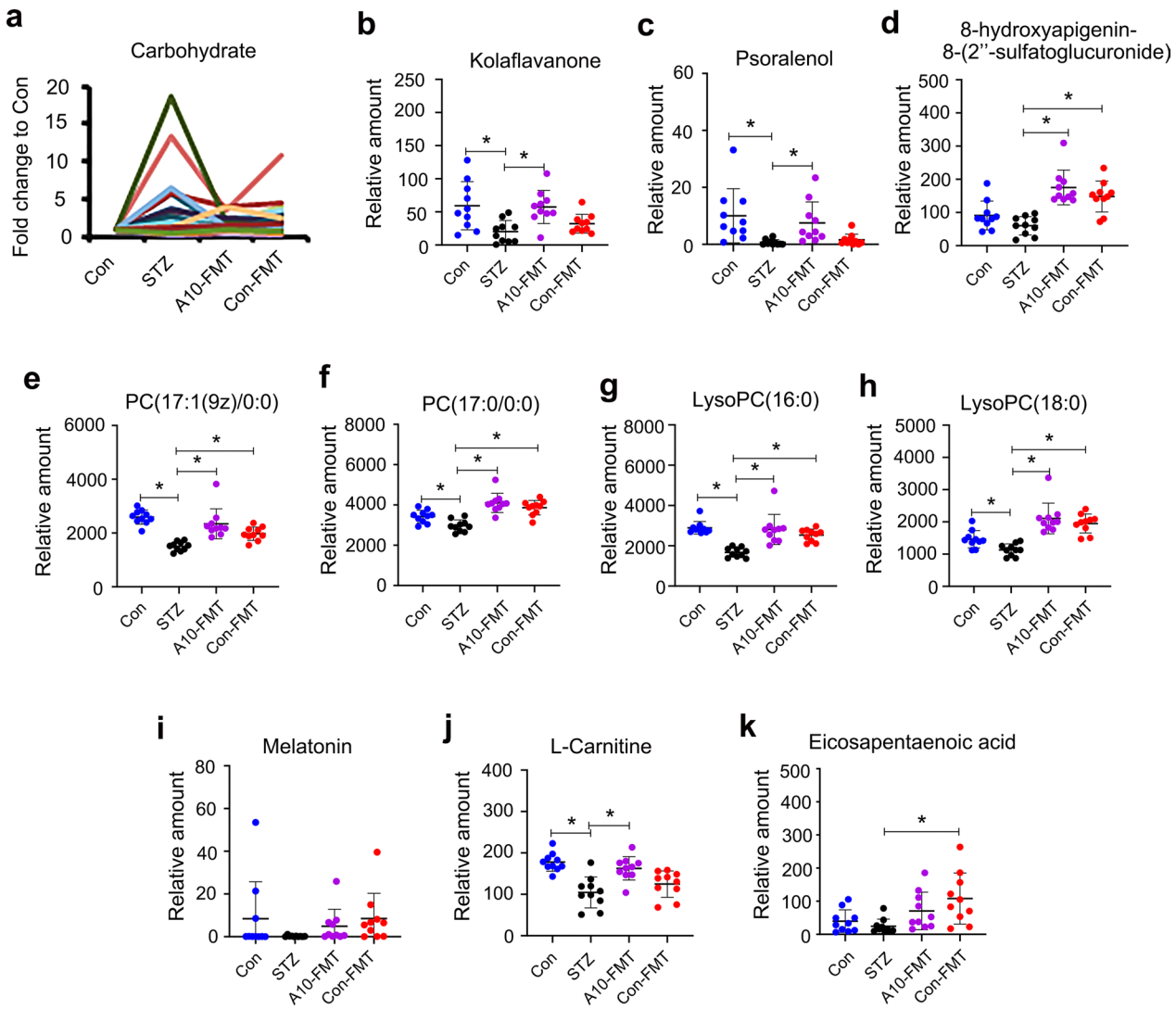

Fig. 3 A10-FMT improved blood metabolism. **a** Blood carbohydrate levels in different treatments. The y-axis represents the fold change compared to control group (Con). The x-axis represents the treatment. **b** Blood flavonoid Kola flavanone levels in different treatments. The y-axis represents the relative amount. The x-axis represents the treatment. *$p < 0.05$. **c** Blood flavonoid Psoralenol levels in different treatments. The y-axis represents the relative amount. The x-axis represents the treatment. *$p < 0.05$. **d** Blood flavonoid 8-hydroxyaplgenin 8-(2″-sulfatoglucuronide) levels in different treatments. The y-axis represents the relative amount. The x-axis represents the treatment. *$p < 0.05$. **e** Blood PC (17:1(9z)/0:0) levels in different treatments. The y-axis represents the relative amount. The x-axis represents the treatment. *$p < 0.05$. **f** Blood PC (17:0/0:0) levels in different treatments. The y-axis represents the relative amount. The x-axis represents the treatment. *$p < 0.05$. **g** Blood LysoPC (16:0) levels in different treatments. The y-axis represents the relative amount. The x-axis represents the treatment. *$p < 0.05$. **h** Blood LysoPC (18:0) levels in different treatments. The y-axis represents the relative amount. The x-axis represents the treatment. *$p < 0.05$. **i** Blood melatonin levels in different treatments. The y-axis represents the relative amount. The x-axis represents the treatment. *$p < 0.05$. **j** Blood L-Carnitine levels in different treatments. The y-axis represents the relative amount. The x-axis represents the treatment. *$p < 0.05$. **k** Blood eicosapentaenoic acid (EPA) levels in different treatments. The y-axis represents the relative amount. The x-axis represents the treatment. *$p < 0.05$. n = 10/group

and DAZL were elevated by A10-FMT (Fig. 4d; Additional file 2: Fig. S4g) which confirmed initiation of the spermatogenesis process. Moreover, testosterone levels were increased by A10-FMT (Fig. 4e and f; Additional file 2: Fig. S4h–k); steroids other than testosterone were increased by A10-FMT while they were decreased by STZ (Fig. 4g and h; Additional file 2: Fig. S4l–p) which together further confirmed initiation of spermatogenesis. Similarly, in the blood, testicular glycerophosphocholines were increased by A10-FMT

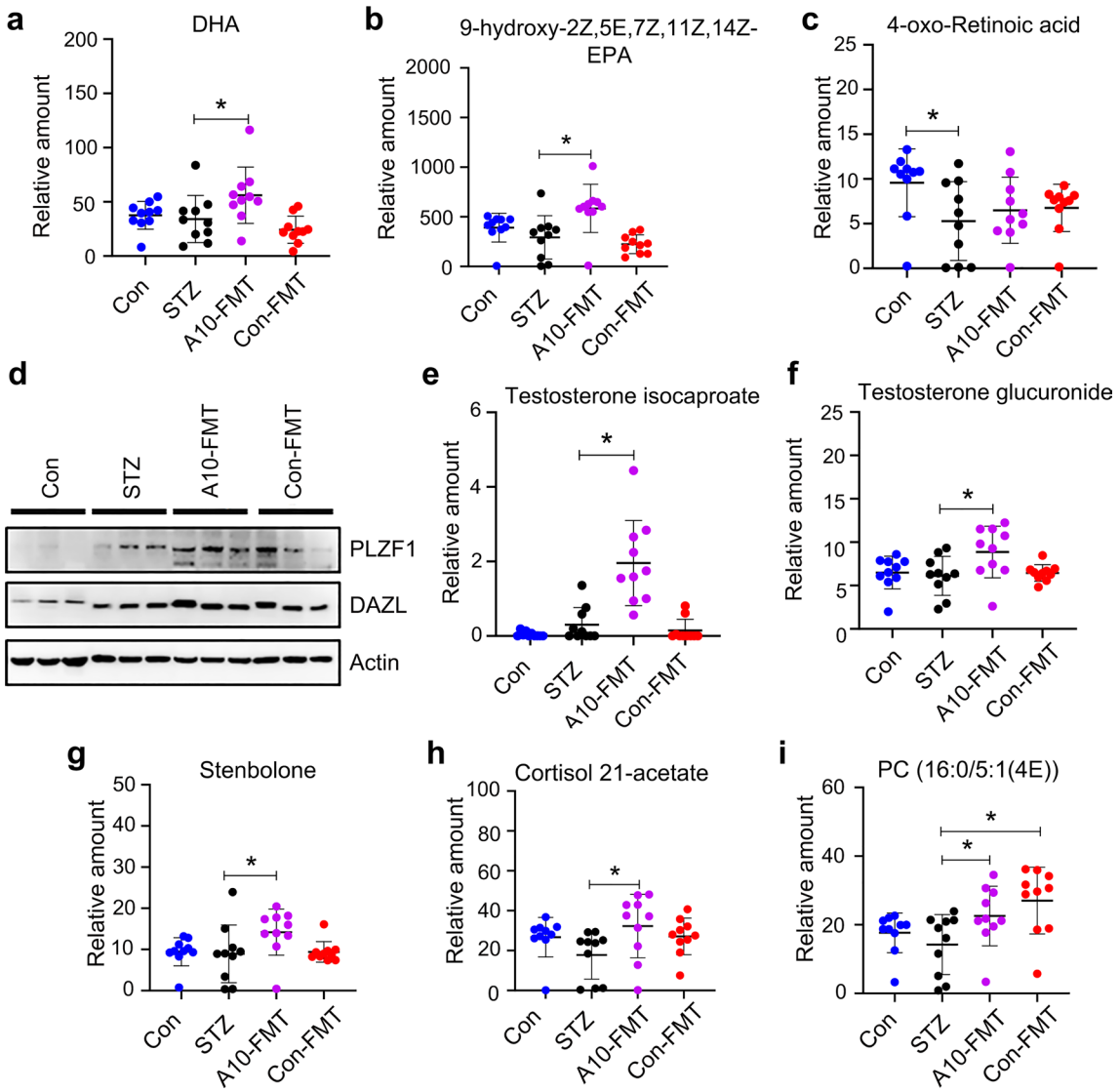

Fig. 4 A10-FMT improved testicular metabolism. **a** Testicular docosahexaenoic acid (DHA) levels in different treatments. The y-axis represents the relative amount. The x-axis represents the treatment. **b** Testicular 9-hydroxy-2Z,5E,7Z,11Z,14Z-Eicosapentaenoic acid levels in different treatments. The y-axis represents the relative amount. The x-axis represents the treatment. *$p < 0.05$. **c** Testicular 4-oxo-Retinoic acid levels in different treatments. The y-axis represents the relative amount. The x-axis represents the treatment. *$p < 0.05$. **d** Testicular protein levels of *PLZF* and *DAZL* in different treatments determined by Western blotting. **e** Testicular testosterone isocaproate levels in different treatments. The y-axis represents the relative amount. The x-axis represents the treatment. *$p < 0.05$. **f** Testicular testosterone glucuronide levels in different treatments. The y-axis represents the relative amount. The x-axis represents the treatment. *$p < 0.05$. **g** Testicular stenbolone levels in different treatments. The y-axis represents the relative amount. The x-axis represents the treatment. *$p < 0.05$. **h** Testicular cortisol 21-acetate levels in different treatments. The y-axis represents the relative amount. The x-axis represents the treatment. *$p < 0.05$. **i** Testicular PC (16:0/5:1(4E)) levels in different treatments. The y-axis represents the relative amount. The x-axis represents the treatment. *$p < 0.05$. n = 10/group

while they were decreased by STZ (Fig. 4i; Additional file 2: Fig. S4q–s). Melatonin metabolite 6-hydroxymelatonin, an active form of melatonin (Maharaj et al. 2005), was increased by A10-FMT (Additional file 2: Fig. S4t).

A10-FMT-improved testicular microenvironment benefited spermatogenesis to improve semen quality

A10-FMT improved the testicular metabolome, especially through increased DHA and EPA which suggested that spermatogenesis should be ameliorated. Spermatogenesis was indeed boosted by A10-FMT

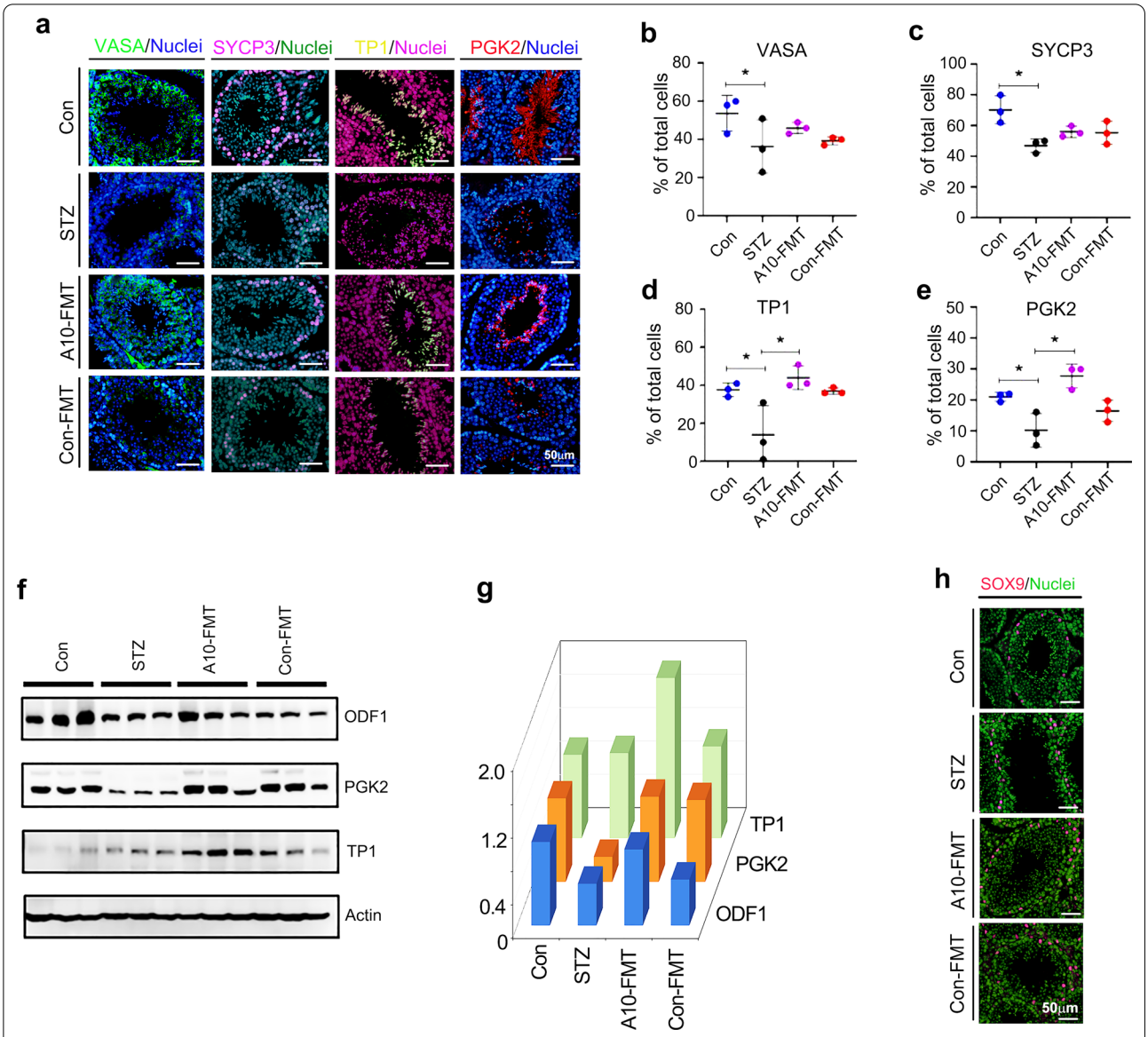

Fig. 5 A10-FMT improved spermatogenesis process. **a** IHF staining of testicular germ cell marker *VASA*, meiosis marker *SYCP3*, sperm protein *PGK2*, and transition protein 1 (*TP1*) in each treatment. Scale bar: 50 μm. n ≥ 3/group. **b** Quantitative data for *VASA* IHF staining. The y-axis represents the percentage of total cell. The x-axis represents the treatment. **p* < 0.05. **c** Quantitative data for *SYCP3* IHF staining. The y-axis represents the percentage of total cell. The x-axis represents the treatment. **p* < 0.05. **d** Quantitative data for *TP1* IHF staining. The y-axis represents the percentage of total cell. The x-axis represents the treatment. **p* < 0.05. **e** Quantitative data for *PGK2* IHF staining. The y-axis represents the percentage of total cells. The x-axis represents the treatment. **p* < 0.05. **f** Western blotting analysis of the proteins of important genes for spermatogenesis in each treatment. n ≥ 3/group. **g** Quantitative data for Western blotting analysis. **h** IHF staining of Sertoli cell marker *SOX9*

(Fig. 5). The protein level (number of positive cells) of germ cell marker *VASA* (*DDX4*) was decreased in T1D animals while increased by A10-FMT (Fig. 5a and b). The protein level (number of positive cells) of the meiosis marker gene *SYCP3* was increased by A10-FMT while reduced by STZ (Fig. 5a and c). The protein level (number of positive cells) of transition protein 1 (*TP1*) was significantly increased by A10-FMT (Fig. 5a and d). The protein level (number of positive cells) of the sperm protein *PGK2* was decreased by STZ while significantly increased by A10-FMT (Fig. 5a and e). Moreover, the protein levels of some of the important genes for spermatogenesis *ODF1*, *PGK2*, *TP1*, *CREM*, *B-MYB*, and *PIWIL1* were determined by Western blotting. It was noteworthy that all these proteins were elevated by A10-FMT (Fig. 5f and g; Additional file 2: Fig.

S5a) which confirmed the IHF data. At the same time the Sertoli cell marker gene *SOX9* was detected by IHF; it was shown that the number of *SOX9* positive cells remained unchanged by STZ or A10-FMT compared to Con (Fig. 5h).

Furthermore, A10-FMT-improved gut microbiota benefited spleen immune function and liver function to strengthen the systemic environment for spermatogenesis

In the current investigation, STZ disrupted spleen function. Spleen RNA-seq data showed that STZ upset spleen gene expression while this was recovered by A10-FMT and/or Con-FMT Additional file 2: Fig. S5b–e). Gene enrichment analysis also showed that functions upset by STZ were reversed by A10-FMT or Con-FMT (Fig. 6a; Additional file 2: Fig. S5b and c). "Adapted immune response", "Complement cascade", and "Platelet activation", "Complement and coagulation cascade", and "hemostasis" functional pathways were enriched for the genes decreased by STZ while they were increased by A10-FMT, which indicated that the immune and vasculature systems may be affected

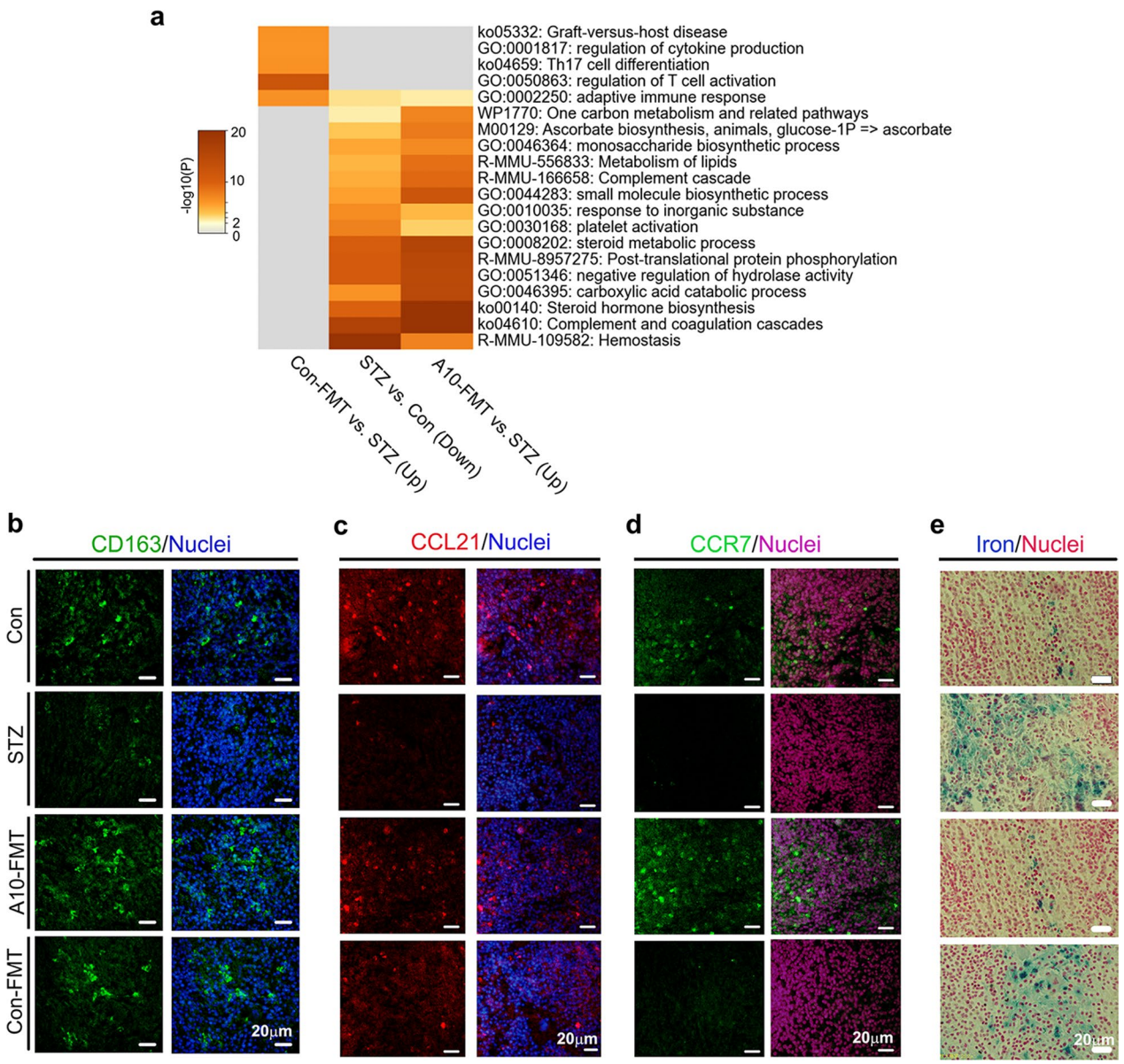

Fig. 6 A10-FMT improved spleen function. **a** Functional enrichment analysis of STZ decreased genes while they were increased by A10-FMT or Con-FMT. **b** IHF staining of *CD163* in spleen tissue. **c** IHF staining of *CCL21* in spleen tissue. **d** IHF staining of *CCR7* in spleen tissue. **e** Perl's Prussian blue stain for ferric iron in spleen tissue. n ≥ 3/group

by STZ and recovered by A10-FMT. The "hemostasis" functional pathway indicated that STZ affected blood supply to the spleen, and it was confirmed by the expression of hemoglobin scavenger receptor (CD163) protein. CD163 is known to play major roles in the clearance and endocytosis of hemoglobin/haptoglobin complexes (Kohyama et al. 2009). STZ decreased CD163 protein levels in the spleen while these were recovered by A10-FMT (Fig. 6b).

A10-FMT improved spleen immune functions. T-cell protein CCL21 and its receptor CCR7 play crucial roles in maintaining the active migratory state of T cells (den Haan et al. 2012). STZ decreased CCL21 protein levels (or positive cells) in the spleen while this was reversed by A10-FMT but not Con-FMT (Fig. 6c). At the same time, the protein levels (or positive cells) of CCR7 were reduced by STZ while they were recovered by A10-FMT but not Con-FMT (Fig. 6d). Moreover STZ increased the levels of iron in the spleen while this was reversed by A10-FMT but not Con-FMT (Fig. 6e). Furthermore, the proliferation and apoptosis status of the spleen was recovered by A10-FMT (Additional file 2: Fig. S5c, d). The protein levels (or the number of positive cells) of cell proliferation marker Ki67 were reduced by STZ while they were increased by A10-FMT (Additional file 2: Fig. S5d). Furthermore, the protein levels of apoptosis markers p53 and Bax were diminished by STZ while they were recovered by A10-FMT (Additional file 2: Fig. S5e).

The liver plays a vital role in glucose metabolism and detoxification and many other functions maintain homeostasis. STZ upset liver function while this was recovered by A10-FMT (Additional file 2: Fig. S6). The liver damage marker alanine aminotransferase (ALT) was increased in the blood while this was decreased by A10-FMT (Additional file 2: Fig. S6a). RNA-seq analysis also showed that STZ disrupted liver functions while this was reversed by A10-FMT and/or Con-FMT (Additional file 2: Fig. S6b–d). KEGG enrichment analysis indicated that liver lipid metabolism was upset by STZ while it was reversed by A10-FMT and/or Con-FMT (Additional file 2: Fig. S6c and d). Furthermore, blood triglyceride (TG) and total cholesterol (TC) levels were increased by STZ while these were reversed by A10-FMT and/or Con-FMT (Additional file 2: Fig. S6e and f).

Antioxidants also play important roles in maintaining systemic functions. Blood total antioxidant capability (T-AOC) level was reduced by STZ while it was recovered by A10-FMT (Additional file 2: Fig. S6g). At the same time the levels of anti-oxidant enzymes SOD and catalase were decreased by STZ while increased by A10-FMT (Additional file 2: Fig. S6h and i). The antioxidant compound GSH was also increased by A10-FMT (Additional file 2: Fig. S6j). At the same time liver apoptosis status was upset by STZ while it was recovered by A10-FMT (Additional file 2: Fig. S6k).

Discussion

Gut dysbiosis is involved in T1D, and male T1D patients pose high possibility to have fertility issues, therefore, gut dysbiosis and male infertility may be correlated. As most male T1D patients may have reproductive issues, it is worth exploring protocols for improving spermatogenesis and male fertility (Liu et al. 2019). Many studies have used different procedures to increase fertility, such as resveratrol and metformin, which are capable of improving semen quality to some extent (Liu et al. 2019; Simas et al. 2017). Very recently, we found that FMT from AOS-improved gut microbiota rescues high fat diet disrupted spermatogenesis. In the current investigation, we found that FMT from AOS-improved gut microbiota (A10-FMT), but not FMT from gut microbiota of control animals (Con-FMT), significantly increased sperm concentration and motility in STZ-induced T1D animals. Moreover, A10-FMT significantly decreased blood glucose and glycogen which suggested that A10-FMT may be supportive management for T1D patients.

Of great interest in the current study was our finding that the small intestine *Lactobacillus* population, which has been shown to have multiple functions in human health (Geng et al. 2021; Lew et al. 2020; Wang et al. 2019; Malik et al. 2018; Maragkoudakis et al. 2010), was increased by A10-FMT but not by Con-FMT. *Lactobacillus plantarum* 299v is reported to decrease systemic inflammation (Malik et al. 2018). *Lactobacillus helveticus* R0052 is known to improve carbohydrate and fatty acid metabolism and reduce lithocholic acid levels (Wang et al. 2019). Lew et al. report that some selected *Lactobacillus* strains improve lipid profiles via activation of energy and lipid metabolism (Lew et al. 2020). *Lactobacillus rhamnosus* GG ATCC53103 and *Lactobacillus plantarum* JL01, can improve growth performance and immunity of piglets via increasing levels of tauroursodeoxycholic acid (TCDA) and docosahexaenoic acid (DHA) (Geng et al. 2021). *Lactobacillus plantarum* PCA 236 has been shown to beneficially modulate fecal microbiota and milk fatty acid composition (Maragkoudakis et al. 2010). These studies indicate that *Lactobacillus* have the capacity to modify the production of polyunsaturated fatty acids such as DHA in animal blood or other organs. *Prevotella* has been found to be inversely related to pancreatic beta cell function, and *Desulfovibrio* to be positively correlated with beta cell function (Knip and Siljander 2016). In the current study, we found *Desulfovibrio* was decreased in the cecum of STZ-induced T1D

animals while A10-FMT and Con-FMT restored its levels; *Prevotella* was increased in the colon of STZ-induced T1D animals while A10-FMT and Con-FMT decreased its levels. As these results show beneficial outcomes, this suggests that FMT could improve gut microbiota.

It is known that n-3 PUFA especially EPA and DHA are important for many aspects of our health, including spermatogenesis (Bunay et al. 2021; Hale et al. 2019; Roqueta-Rivera et al. 2010). Moreover, it has also been shown that DHA supplementation can fully restore fertility and spermatogenesis in male mice (Roqueta-Rivera et al. 2010). Meanwhile, Gallardo et al. report that a high fat diet decreases testicular DHA levels, which may be related to the production of dysfunctional spermatozoa (Bunay et al. 2021). The identification of beneficial n-3 PUFAs in this study was enlightening; we suggest that DHA and EPA were increased by A10-FMT in the blood and testes which was correlated with the increase in *Lactobacillus* in the small intestine following A10-FMT treatment. The current and previous studies have demonstrated that *Lactobacillus spp.* have the potential to improve DHA levels, which is important for aspects of health, including improvements in spermatogenesis. Furthermore, testosterone is a strategic player in spermatogenesis, and approximately 94.4% of diabetes cases are associated with hypotestosteronemia. Moreover, the incidence of sexual and reproductive dysfunction in diabetic patients is 5- to 10-fold higher than that in nondiabetic individuals (Liu et al. 2019). In current study, A10-FMT increased the testicular testosterone levels, which may account for the improvement of spermatogenesis and semen quality.

T1D is an immune related disease, and perturbations in the gut microbiota can impair the functions of immune cells and vice-versa (Abdellatif and Sarvetnick 2019). Such dysbiosis is often detected in T1D subjects, especially those with an adverse immunoresponse (Abdellatif and Sarvetnick 2019). Recently, it has been established that the gut microbiota is involved in spleen development and function (Carsetti et al. 2020; Rosado et al. 2018); and a gut-spleen interaction (axis) has been identified. The spleen plays vital roles in systemic immune function (Carsetti et al. 2020; Rosado et al. 2018). Moreover, the spleen plays important roles in iron homeostasis through the resorption of effete erythrocytes and the subsequent return of iron to the circulation. Free iron has the potential to become cytotoxic when electron exchange with oxygen is unrestricted and catalyzes the production of reactive oxygen species. Therefore, the balance of iron in the spleen and circulation is very important for health (Soares and Hamza 2016; Gammella et al. 2014; Kohyama et al. 2009). In the current study, we found that STZ-induced T1D disrupted spleen function while A10-FMT rescued it through the improvement of immune cell function and iron levels. Free iron levels in the spleen or liver may potentially become cytotoxic as they can catalyze the production of reactive oxygen species (ROS; Soares and Hamza 2016). A10-FMT beneficially decreased spleen iron levels, reduced apoptosis protein levels, and increased cell proliferation marker ki67 levels, all of which indicate improvements in spleen function (Kohyama et al. 2009). Macrophages, indispensable immune cells, also play important roles in the regulation of spleen iron levels (Soares and Hamza 2016; Gammella et al. 2014), which further suggests that A10-FMT improves spleen immune function. All the data suggested that A10-FMT benefited spleen functions to assist with systemic immune functions since T1D is an important immune related disease (Mariño et al. 2017). This improvement in spleen function may support systemic health and spermatogenesis.

The main characteristic of T1D is hyperglycemia which can induce oxidative stress, increase endoplasmic reticulum stress, and impair mitochondrial function (Maresch et al. 2018). We found that STZ-induced T1D decreased T-AOC level and the levels of some antioxidant enzymes, such as SOD, while A10-FMT restored them. We also detected that STZ-induced T1D caused liver damage through increasing ALT levels, while A10-FMT recovered it. At the same time A10-FMT improved liver function by modulating the apoptotic status in liver cells. All the data suggested that A10-FMT had a strong capacity to improve levels of systemic antioxidants to benefit spermatogenesis since T1D induced hyperglycemia causes systemic oxidative stress (Maresch et al. 2018).

Conclusion

In our animal model, STZ-induced T1D disrupted spermatogenesis to diminish semen quality through decreasing sperm concentration and sperm motility. Most importantly, STZ-induced T1D caused gut dysbiosis. A10-FMT and Con-FMT decreased blood glucose levels and improved gut microbiota through the reduction of "harmful" microbes and increase in "beneficial" microbes. Most importantly, A10-FMT enhanced specific beneficial microbiota such *Lactobacillus* to increase the production of n-3 PUFA, such as DHA and EPA, to ameliorate spermatogenesis and semen quality while Con-FMT did not. Moreover, A10-FMT specifically improved spleen and liver function to promote sperm development and increase semen quality. Thus, AOS improved gut microbiota may support the improvement of semen quality and male fertility in T1D patients in the future.

Abbreviations

AOS: Alginate oligosaccharide; CASA: Computer-assisted sperm assay; DHA: Docosahexaenoic acid; DM: Diabetes mellitus; FMT: Fecal microbiota transplantation; EPA: Eicosapentaenoic acid; KEGG: Kyoto Encyclopedia of Genes and Genomes; PUFA: Polyunsaturated fatty acid; STZ: Streptozotocin; T1D: T-AOC: total antioxidant capability; type 1 diabetes; TC: Total cholesterol; TCDA: Tauroursodeoxycholic acid; TG: Triglyceride.

Supplementary Information

The online version contains supplementary material available at https://doi.org/10.1186/s10020-022-00473-w.

Additional file 1: Table S1. Primary antibody information.

Additional file 2: Fig. S1. Body weight and gut microbiota changes (STZ vs. Con). **a** Animal bodyweight. The y-axis represents the body weight (g). The x-axis represents the age (weeks). **b** Blood insulin levels. The y-axis represents the concentration (mIU/L). The x-axis represents the treatment. **c** The alpha index of the small intestine microbiota (Chao index). The y-axis represents the relative amount. The x-axis represents the treatment. **d** The beta index of small intestinal microbiota. The y-axis represents the relative amount. The x-axis represents the treatment. **e** PLS-DA (OTU) of small intestine microbiota in STZ and Con groups. **f** Small intestine microbiota levels at the genus level in STZ and Con groups. The y-axis represents the relative amount (%). The x-axis represents the individual microbiota. **g** The alpha index of the cecum microbiota (Chao index). The y-axis represents the relative amount. The x-axis represents the treatment. **h** The beta index of cecum microbiota. The y-axis represents the relative amount. The x-axis represents the treatment. **i** PLS-DA (OTU) of cecum microbiota in STZ and Con groups. **j** Cecum microbiota levels at the genus level in STZ and Con groups. The y-axis represents the relative amount (%). The x-axis represents the individual microbiota. **k** The alpha index of the colon microbiota (Chao index). The y-axis represents the relative amount. The x-axis represents the treatment. **l** The beta index of colon microbiota. The y-axis represents the relative amount. The x-axis represents the treatment. **m** PLS-DA (OTU) of colon microbiota in STZ and Con groups. **n** Colon microbiota levels at the genus level in STZ and Con groups. The y-axis represents the relative amount (%). The x-axis represents the individual microbiota. **Fig. S2. a** PLS-DA (OTU) of cecum microbiota in STZ, A10-FMT, and Con-FMT groups. **b** Cecum microbiota levels at the genus level in STZ, A10-FMT, and Con-FMT groups. The y-axis represents the relative amount (%). The x-axis represents the treatments. Different colors represent different microbiota. **c** Cladogram of the LEfSe determining the cecum microbiota difference in abundance. **d** Changed microbiota in the cecum. The y-axis represents the relative amount at the genus level. The x-axis represents the treatment. *$p < 0.05$. **e** PLS-DA (OTU) of colon microbiota in STZ, A10-FMT, and Con-FMT groups. **f** Colon microbiota levels at the genus level in STZ, A10-FMT, and Con-FMT groups. The y-axis represents the relative amount (%). The x-axis represents the treatments. Different colors represent different microbiota. **g** Cladogram of the LEfSe determining the difference in abundance of colon microbiota. **h** Changed microbiota in the colon. The y-axis represents the relative amount at the genus level. The x-axis represents the treatment. *$p < 0.05$. **Fig. S3.** Blood metabolism changes. **a** Blood flavonoid Malvidin 3-O-(6-O-(4-O-feruloyl-alpha-rhamnopyranosyl)-beta-glucopyranoside)-5-beta-glucopy -ranoside levels. The y-axis represents the relative amount (%). The x-axis represents the treatments. **b** Blood glycerophosphocholine levels in different treatments. The y-axis represents the fold change compared to control group (Con). The x-axis represents the treatment. **c** Blood LysoPC (15:0) levels. The y-axis represents the relative amount (%). The x-axis represents the treatments. **d** Blood LysoPC [18:1(9z)] levels. The y-axis represents the relative amount (%). The x-axis represents the treatments. **e** Blood LysoPC [22:6(4Z,7Z,10Z,13Z,16Z,19Z)] levels. The y-axis represents the relative amount (%). The x-axis represents the treatments. **f** Blood PE [22:2(13Z,16Z)/0:0] levels. The y-axis represents the relative amount (%). The x-axis represents the treatments. **g** Blood PE (22:0/0:0) levels. The y-axis represents the relative amount (%). The x-axis represents the treatments. **h** Blood PE [22:1(11Z)/0:0] levels. The y-axis represents the relative amount (%). The x-axis represents the treatments. **i** Blood LysoPE [0:0/24:6(6Z,9Z,12Z,15Z,18Z,21Z)] levels. The y-axis represents the relative amount (%). The x-axis represents the treatments. **Fig. S4.** Testicular metabolite changes. **a** Testicular 4,8,12,15,18-eicosapentaenoic acid levels. The y-axis represents the relative amount (%). The x-axis represents the treatments. **b** Testicular EPA in different treatments. The y-axis represents the relative amount. The x-axis represents the treatment. *$p < 0.05$. **c** Testicular retinoids levels in different treatments. The y-axis represents the fold change compared to the control group (Con). The x-axis represents the treatment. **d** Testicular retinol levels. The y-axis represents the relative amount (%). The x-axis represents the treatments. **e** Testicular 9-cis-retinal levels in different treatments. The y-axis represents the relative amount. The x-axis represents the treatment. *$p < 0.05$. **f** Testicular retinyl ester levels. The y-axis represents the relative amount (%). The x-axis represents the treatments. **g** Quantitative data for Western blotting analysis in Fig. 4d. **h** Testicular testosterone levels in different treatments. The y-axis represents the fold change compared to control group (Con). The x-axis represents the treatment. **i** Testicular testosterone propionate levels. The y-axis represents the relative amount (%). The x-axis represents the treatments. **j** Testicular testosterone acetate levels. The y-axis represents the relative amount (%). The x-axis represents the treatments. **k** Testicular 7alpha-hydroxytestosterone levels in different treatments. The y-axis represents the relative amount. The x-axis represents the treatment. *$p < 0.05$. **l** Testicular steroids levels in different treatments. The y-axis represents the fold change compared to control group (Con). The x-axis represents the treatment. **m** Testicular 3b,17b-Dihydroxyetiocholane levels. The y-axis represents the relative amount (%). The x-axis represents the treatments. **n** Testicular 5-Androstene-3b,16b,17a-triol levels. The y-axis represents the relative amount (%). The x-axis represents the treatments. **o** Testicular 3beta,17alpha,21-Trihydroxy-pregnenone levels. The y-axis represents the relative amount (%). The x-axis represents the treatments. **p** Testicular asterogenol levels. The y-axis represents the relative amount (%). The x-axis represents the treatments. **q** Testicular PCs levels in different treatments. The y-axis represents the fold change compared to the control group (Con). The x-axis represents the treatment. **r** Testicular) PC(4:0/18:1(9Z) level. The y-axis represents the relative amount (%). The x-axis represents the treatments. **s** Testicular PC (8:0/8:0) levels. The y-axis represents the relative amount (%). The x-axis represents the treatments. **t** Testicular 6-hydroxymelatonin levels in different treatments. The y-axis represents the relative amount. The x-axis represents the treatment. *$p < 0.05$. **Fig. S5.** Additional data for testis and spleen. **a** Western blotting analysis of the proteins of some important genes for spermatogenesis in each treatment. n≥3/group. **b** PCA for RNA-seq analysis of spleen. **c** The functional enrichment analysis of STZ increased genes while these were decreased by A10-FMT or Con-FMT. **d** IHF staining of *ki67* in the spleen. **e** Western blotting analysis of *p53*, *Bax* and *Bcl-xl* in the spleen. **Fig. S6.** A10-FMT improved liver function and systemic anti-oxidative capability. **a** Blood alanine aminotransferase (ALT) levels. The y-axis represents the relative amount (%). The x-axis represents the treatments. **b** PCA for RNA-seq analysis of liver. **c** The functional enrichment analysis of STZ decreased genes while these were increased by A10-FMT or Con-FMT in the liver. **d** The functional enrichment analysis of STZ increased genes while these were decreased by A10-FMT or Con-FMT in the liver. **e** Blood total triglyceride (TG) levels. The y-axis represents the relative amount (%). The x-axis represents the treatments. **f** Blood total cholesterol (TC) levels. The y-axis represents the relative amount (%). The x-axis represents the treatments. **g** Blood total antioxidant capability (T-AOC) levels. The y-axis represents the relative amount (%). The x-axis represents the treatments. **h** Blood total SOD levels. The y-axis represents the relative amount (%). The x-axis represents the treatments. **i** Blood catalase levels. The y-axis represents the relative amount (%). The x-axis represents the treatments. **j** Blood glutathione (GSH) levels. The y-axis represents the relative amount (%). The x-axis represents the treatments. **k** Western blotting analysis of *Bax* and *Bcl-xl* in the liver.

Additional file 3: Data Set 1. Blood metabolites raw data.

Additional file 4: Data Set 2. Testicular metabolites raw data.

Acknowledgements
We thank the investigators and staff of The Beijing Genomics Institute (BGI) and Shanghai LUMING Biotechnology CO., LCD for technical support.

Author contributions
YH, YF, XY, LC, RZ, and XT performed the experiments and analyzed the data. YZ, HZ, WS, QS, ZS, and YR designed and supervised the study. YZ, and HZ wrote the manuscript. All the authors edited the manuscript and approved the final manuscript.

Funding
This study was supported by the National Natural Science Foundation of China (Grant No. 31772408 and 32070536 to YZ; 31672428 to HZ).

Availability of data and materials
Liver and spleen RNA-seq raw data were deposited in NCBI's Gene Expression Omnibus under accession number GSE184021 and GSE184023, respectively. The microbiota raw sequencing data generated in this study has been uploaded to the NCBI SRA database with the accession number PRJNA759114 (small intestine), PRJNA759089 (cecum), and PRJNA759063 (colon).

Declarations

Ethics approval and consent to participate
The study was approved by the Institutional Animal Care and Use Committee of Institute of Animal Sciences of Chinese Academy of Agricultural Science and performed following the relevant guidelines and regulations.

Consent for publication
Not applicable.

Competing interests
The authors declare no competing interests.

Author details
[1]State Key Laboratory of Animal Nutrition, Institute of Animal Sciences, Chinese Academy of Agricultural Sciences, Beijing 100193, People's Republic of China. [2]College of Life Sciences, Qingdao Agricultural University, Qingdao 266109, People's Republic of China. [3]College of Science, Health, Engineering and Education, Murdoch University, Perth 6150, Australia. [4]College of Veterinary Medicine, Qingdao Agricultural University, Qingdao 266109, People's Republic of China. [5]Fertility Preservation Lab, Reproductive Medicine Center, Guangdong Second Provincial General Hospital, Guangzhou 510317, People's Republic of China. [6]Urology Department, Shenzhen University General Hospital, Shenzhen 518055, People's Republic of China.

Received: 12 January 2022 Accepted: 11 April 2022
Published online: 25 April 2022

References

Abdellatif AM, Sarvetnick NE. Current understanding of the role of gut dysbiosis in type 1 diabetes. J Diabetes. 2019;11(8):632–44.
Allegretti JR, Mullish BH, Kelly C, Fischer M. The evolution of the use of faecal microbiota transplantation and emerging therapeutic indications. Lancet. 2019;394(10196):420–31.
Bárcena C, Valdés-Mas R, Mayoral P, Garabaya C, Durand S, Rodríguez F, et al. Healthspan and lifespan extension by fecal microbiota transplantation into progeroid mice. Nat Med. 2019;25:1234–42.
Barkabi-Zanjani S, Ghorbanzadeh V, Aslani M, Ghalibafsabbaghi A, Chodari L. Diabetes mellitus and the impairment of male reproductive function: possible signaling pathways. Diabetes Metab Syndr. 2020;14(5):1307–14.
Bowles J, Knight D, Smith C, Wilhelm D, Richman J, Mamiya S, et al. Retinoid signaling determines germ cell fate in mice. Science. 2006;312:596–600.
Brunse A, Martin L, Rasmussen TS, Christensen L, Cilieborg MS, Wiese M, et al. Effect of fecal microbiota transplantation route of administration on gut colonization and host response in preterm pigs. ISME J. 2019;13:720–33.
Bunay J, Gallardo L, Torres-Fuentes JL, Aguirre-Arias MV, Orellana R, Sepúlveda N, et al. A decrease of docosahexaenoic acid in testes of mice fed a high-fat diet is associated with impaired sperm acrosome reaction and fertility. Asian J Androl. 2021;23(3):306–13.
Carsetti R, Sabatino AD, Rosado MM, Cascioli S, Mortari EP, Milito C, Grimsholm O, et al. Lack of gut secretory immunoglobulin A in memory B-cell dysfunction-associated disorders: a possible gut-spleen axis. Front Immunol. 2020;10:2937.
Chu M, Zhao Y, Yu S, Hao Y, Zhang P, Feng Y, et al. MicroRNA-221 may be involved in lipid metabolism in mammary epithelial cells. Int J Biochem Cell Biol. 2018;97:118–27.
de Groot P, Nikolic T, Pellegrini S, Sordi V, Imangaliyev S, Rampanelli E, et al. Faecal microbiota transplantation halts progression of human new- onset type 1 diabetes in a randomized controlled trial. Gut. 2021;70(1):92–105.
den Haan JM, Mebius RE, Kraal G. Stromal cells of the mouse spleen. Front Immunol. 2012;3:201.
Ding N, Zhang X, Zhang X, Jing J, Liu S, Mu Y, et al. Impairment of spermatogenesis and sperm motility by the high-fat diet-induced dysbiosis of gut microbes. Gut. 2020;69:1608–19.
Gammella E, Buratti P, Cairo G, Recalcati S. Macrophages: central regulators of iron balance. Metallomics. 2014;6:1336–45.
Geng T, He F, Su S, Sun K, Zhao L, Zhao Y, et al. Probiotics *Lactobacillus rhamnosus* GG ATCC53103 and *Lactobacillus plantarum* JL01 induce cytokine alterations by the production of TCDA, DHA, and succinic and palmitic acids, and enhance immunity of weaned piglets. Res Vet Sci. 2021;137:56–67.
Glazer CH, Bonde JP, Giwercman A, Vassard D, Pinborg A, Schmidt L, et al. Risk of diabetes according to male factor infertility: a register-based cohort study. Hum Reprod. 2017;32(7):1474–81.
Griswold MD. Spermatogenesis: the commitment to meiosis. Physiol Rev. 2016;96:1–17.
Gülden E, Wong FS, Wen L. The gut microbiota and type 1 diabetes. Clin Immunol. 2015;159(2):143–53.
Hale BJ, Fernandez RF, Kim SQ, Diaz VD, Jackson SN, Liu L, et al. Acyl-CoA synthetase 6 enriches seminiferous tubules with the n-3 fatty acid docosahexaenoic acid and is required for male fertility in the mouse. J Biol Chem. 2019;294(39):14394–405.
Jangir RN, Jain GC. Diabetes mellitus induced impairment of male reproductive functions: a review. Curr Diabetes Rev. 2014;10(3):147–57.
Knip M, Honkanen J. Modulation of type 1 diabetes risk by the intestinal microbiome. Curr Diabetes Rep. 2017;17(11):105.
Knip M, Siljander H. The role of the intestinal microbiota in type 1 diabetes mellitus. Nat Rev Endocrinol. 2016;12(3):154–67.
Kohyama M, Ise W, Edelson BT, Wilker PR, Hildner K, Mejia C, et al. Role for Spi-C in the development of red pulp macrophages and splenic iron homeostasis. Nature. 2009;457:318–21.
Kostic AD, Gevers D, Siljander H, Vatanen T, Hyötyläinen T, Hämäläinen A, et al. The dynamics of the human infant gut microbiome in development and in progression towards type 1 diabetes. Cell Host Microbe. 2015;17(2):260–73.
La Vignera S, Condorelli RA, Di Mauro M, Lo Presti D, Mongioì LM, Russo G, et al. Reproductive function in male patients with type 1 diabetes mellitus. Andrology. 2015;3(6):1082–7.
Lengqvist J, Mata De Urquiza A, Bergman AC, Willson TM, Sjövall J, Perlmann T, et al. Polyunsaturated fatty acids including docosahexaenoic and arachidonic acid bind to the retinoid X receptor alpha ligand-binding domain. Mol Cell Proteomics. 2004;3:692–703.
Lew L, Hor Y, Jaafar M, Lau A, Lee B, Chuah L, et al. Lactobacillus Strains Alleviated Hyperlipidemia and Liver Steatosis in Aging Rats via Activation of AMPK. Int J Mol Sci. 2020;21(16):5872.
Li WZ, Stirling K, Yang JJ, Zhang L. Gut microbiota and diabetes: from correlation to causality and mechanism. World J Diabetes. 2020;11(7):293–308.
Liu Y, Yang Z, Kong D, Zhang Y, Yu W, Zha W. Metformin ameliorates testicular damage in male mice with streptozotocin-induced type 1 diabetes through the PK2/PKR pathway. Oxid Med Cell Longev. 2019;2019:5681701.
Maharaj DS, Maharaj H, Antunes EM, Maree DM, Nyokong T, Glass BD, et al. 6-Hydroxymelatonin protects against quinolinic-acid-induced oxidative neurotoxicity in the rat hippocampus. J Pharm Pharmacol. 2005;57(7):877–81.
Malik M, Suboc TM, Tyagi S, Salzman N, Wang J, Ying R, et al. Lactobacillus Plantarum 299v supplementation improves vascular endothelial function

and reduces inflammatory biomarkers in men with stable coronary artery disease. Circ Res. 2018;123(9):1091–102.
Maragkoudakis PA, Mountzouris KC, Rosu C, Zoumpopoulou G, Papadimitriou K, Dalaka E, et al. Feed supplementation of *Lactobacillus plantarum* PCA 236 modulates gut microbiota and milk fatty acid composition in dairy goats—a preliminary study. Int J Food Microbiol. 2010;141(Suppl 1):S109–16.
Maresch CC, Stute DC, Alves MG, Oliveira PF, de Kretser DM, Linn T. Diabetes-induced hyperglycemia impairs male reproductive function: a systematic review. Hum Reprod Update. 2018;24(1):86–105.
Mariño E, Richards JL, McLeod KH, Stanley D, Yap YA, Knight J, et al. Gut microbial metabolites limit the frequency of autoimmune T cells and protect against type 1 diabetes. Nat Immunol. 2017;18(5):552–62.
Neuman V, Cinek O, Funda DP, Hudcovic T, Golias J, Kramna L, et al. Human gut microbiota transferred to germ-free NOD mice modulate the progression towards type 1 diabetes regardless of the pace of beta cell function loss in the donor. Diabetologia. 2019;62(7):1291–6
Roqueta-Rivera M, Stroud CK, Haschek WM, Akare SJ, Segre M, Brush RS, et al. Docosahexaenoic acid supplementation fully restores fertility and spermatogenesis in male delta-6 desaturase-null mice. J Lipid Res. 2010;51(2):360–7.
Rosado MM, Aranburu A, Scarsella M, Cascioli S, Giorda E, Del Chierico F, Mortera SL, et al. Spleen development is modulated by neonatal gut microbiota. Immunol Lett. 2018;199:1–15.
Simas JN, Mendes TB, Paccola CC, Vendramini V, Miraglia SM. Resveratrol attenuates reproductive alterations in type 1 diabetes-induced rats. Int J Exp Pathol. 2017;98(6):312–28.
Soares MP, Hamza I. Macrophages and iron metabolism. Immunity. 2016;44:492–504.
Wang Q, Lv L, Jiang H, Wang K, Yan R, Li Y, et al. Lactobacillus helveticus R0052 alleviates liver injury by modulating gut microbiome and metabolome in D-galactosamine-treated rats. Appl Microbiol Biotechnol. 2019;103(23–24):9673–86.
Wen L, Ley RE, Volchkov PY, Stranges PB, Avanesyan L, Stonebraker AC, et al. Innate immunity and intestinal microbiota in the development of Type 1 diabetes. Nature. 2008;455(7216):1109–13.
Wolf G. Is 9-cis-retinoic acid the endogenous ligand for the retinoic acid-X receptor? Nutr Rev. 2006;64:532–8.
Yurtdaş G, Akdevelioğlu Y. A new approach to polycystic ovary syndrome: the gut microbiota. J Am Coll Nutr. 2019;12:1–12.
Zhang P, Feng Y, Li L, Ge W, Yu S, Hao Y, et al. Improvement in sperm quality and spermatogenesis following fecal microbiota transplantation from alginate oligosaccharide dosed mice. Gut. 2021a;70:222–5.
Zhang C, Xiong B, Chen L, Ge W, Yin S, Feng Y, et al. Rescue of male fertility following fecal microbiota transplantation from alginate oligosaccharide dosed mice. Gut. 2021b;70(11):2213–5.
Zhang T, Sun P, Geng Q, Fan H, Gong Y, Hu Y, Shan L, Sun Y, Shen W, Zhou Y. Disrupted spermatogenesis in a metabolic syndrome model: the role of vitamin A metabolism in the gut–testis axis. Gut. 2022;71(1):78–87.
Zhao Y, Zhang P, Ge W, Feng Y, Li L, Sun Z, et al. Alginate oligosaccharides improve germ cell development and testicular microenvironment to rescue busulfan disrupted spermatogenesis. Theranostics. 2020;10:3308–24.

Publisher's Note